



## Spectroscopic investigation of Dione' surface using Cassini VIMS images

F. Scipioni<sup>1</sup>, A. Coradini<sup>2</sup>, F. Tosi<sup>2</sup>, F. Capaccioni<sup>1</sup>, P. Cerroni<sup>1</sup>, G. Filacchione<sup>1</sup>,  
C. Federico<sup>3</sup>, and the Cassini VIMS Team

<sup>1</sup> INAF-IASF, Via del Fosso del Cavaliere 100, 00133 Rome, Italy

<sup>2</sup> INAF-IFSI, Via del Fosso del Cavaliere 100, 00133 Rome, Italy

<sup>3</sup> Università degli studi di Perugia, Dipartimento di Scienze della Terra, Piazza Università  
- 06123 Perugia  
e-mail: francesca.scipioni@ifsi-roma.inaf.it

### Abstract.

Dione is the second largest inner moon of Saturn. It is composed primarily of water ice ( $\rho = 1.475 \pm 0.003 \text{ g/cm}^3$ ), and is the third densest of Saturn's moons (after Enceladus and Titan). This satellite was observed several times by the Cassini spacecraft in its nominal and extended mission from 2004 to 2008. The VIMS (Visual and Infrared Mapping Spectrometer) instrument onboard the Cassini Orbiter is able to acquire hyperspectral image cubes in the overall spectral range from 0.35 to 5.1  $\mu\text{m}$ . We select 76 VIMS cubes of Dione in the IR range between 0.85 and 5.1  $\mu\text{m}$ , choosing those data which show at the same time: a spatial resolution better than 100 km, a phase angle smaller than 40° and a good S/N ratio. We apply Spectral Angle Mapper (SAM) clustering technique to the spectra of the surface in order to emphasize the presence of different terrain units; then we investigate the compositional and photometric characteristics of these terrain types. In this work we choose the two cubes with the highest spatial resolution among the whole data set to show classification results.

**Key words.** Dione – Cassini mission – Cassini VIMS – Saturn

### 1. Introduction

With a diameter of 1122 km, Dione is the second largest inner moon of Saturn and the third densest after Enceladus and Titan ( $\rho=1.475 \pm 0.003 \text{ g/cm}^3$ ). It was discovered in 1684 by Giovanni Cassini and orbits Saturn at a distance of 377,396 km in coincidence with the outer part of E ring, whose main source is attributed to Enceladus' cryovolcanism. The Voyager spacecraft observed Dione in 1980

showing a complex surface structure, second just to Enceladus. Afterwards this object was observed by the Cassini spacecraft in both its nominal and extended mission from 2004 to 2010. Dione' surface is composed primarily by water ice with minor abundances of volatiles such as CO<sub>2</sub> and CN (Clark et al., 2008). Dione's terrain can be divided in some distinct classes. On the basis of Voyager data, Smith et al. (1981) identified two different units: heavily cratered terrain and less cratered plains. Subsequently Plescia & Boyce (1982)

---

*Send offprint requests to:* F. Scipioni

**Table 1.** VIMS Cubes observations parameters

Cube Name	Seq./Session	Obs. date	Exp. time [ms/px]	Dist. from target center [km]	Mean phase angle [deg]	Mean spatial resolution [km/px]
V1507743872_1.QUB	S15/DIONE205	05 OCT 16	120	18566.2	20.4	7.14
V1507744146_1.QUB	S15/DIONE205	05 OCT 16	120	16070.5	19.9	6.33

subdivided the plains in lobate deposits and bright wispy material, on the basis of impact craters frequency. Most of Dione' surface is covered by heavily cratered terrains, located mainly in the trailing hemisphere and crossed by high-albedo wispy streaks. The origin of dark material that covers the heavily cratered terrains is still unknown, while wispy units are likely tectonic features (Wagner et al., 2006). The presence of such structures lets suppose that Dione experienced geologic activity in the past. However, from recent Cassini data, no active regions have been observed to date. Stephan et al. (2010) developed a more accurate geological classification of Dione' surface, identifying four geological units:

- densely cratered plains (*dcp*), characterized by high albedo and high impact frequency, with craters of different size and degradation state. Craters production reaches the equilibrium on this unit, making it the oldest Dione' surface type.
- Smooth plains (*sp*) on Dione have small crater density and are identified with Plescia's less cratered plans.
- Fractured cratered plains (*fcpl*) correspond to the large tectonic features and wispy terrain, associated with parallel deep scarps and troughs.
- Impact crater material is subdivided in three subclasses (*C1*, *C2* and *C3*), depending on craters' degree of degradation. *C3* class is representative of youngest craters, while *C1* is indicative of the highest degree of degradation.

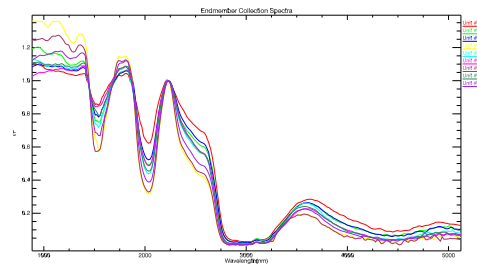


**Fig. 1.** End-member pixels' spectra used to drive Spectral Angle Mapper (SAM) classification method. Different colors identify each reference unit



**Fig. 2.** Cubes V1507743872\_1.QUB (on the left) and V1507744146\_1.QUB (on the right) show the highest spatial resolution in the explored data set. Light stripe in both images is the so called *Padua Chasmata*, classified as a wispy terrain (Plescia & Boyce 1982)

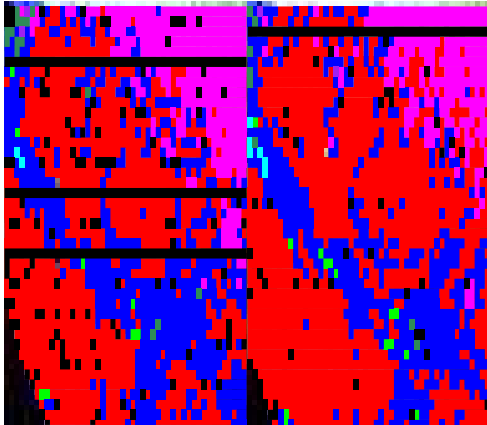


**Fig. 3.** Pixel classification of the cubes V1507743872.1.QUB (on the left) and V1507744146.1.QUB (on the right) based on the supervised method Spectral Angle Mapper (SAM). Different terrain units are represented by the same colors used to identify end-member pixels in Fig. 1. Black pixel indicate those pixels we decided to not include in the classification because their spectra show unremovable spikes or other faults.

## 2. Data set and analysis

The *Visual and Infrared Mapping Spectrometer* (VIMS) instrument onboard the Cassini Orbiter is able to acquire hyperspectral image cubes in the overall spectral range from 0.35 to 5.1  $\mu\text{m}$ , using two separate subsystems devoted to the VIS and IR range, respectively. We select 76 VIMS cubes of Dione in the IR range between 0.85 and 5.1  $\mu\text{m}$ , selecting those data which show at the same time: a spatial resolution better than 100 km, a phase angle smaller than 40° and a good S/N ratio (essentially driven by exposure time). We normalize all spectra at  $\lambda=2.232 \mu\text{m}$  in order to minimize photometric effects due to different observation conditions. We apply a clustering technique to the spectra of each cube based on the supervised method *Spectral Angle Mapper* (SAM) in order to emphasize the presence of spectral units.

For each terrain type we chose one pixel in the image, whose infrared spectrum is used to drive the SAM classification. We

begin by selecting two end-member pixels, one representing a dark terrain and the other one indicative of a wispy terrain. Since two pixels are not enough to properly represent all terrain types as seen in various VIMS cubes, we added further pixels from different cubes until all pixels of the dataset were classified in a terrain unit. In particular, we selected nine different reference pixels, whose spectra are shown in Fig. 1, identified by different colors. In the SAM method applied to remote sensing data, each spectrum is represented by a vector in the  $n$ -dimensional coordinate system, where  $n$  is the number of spectral channels. In the case of VIMS-IR,  $n = 256$ . In order to compare the spectra of the target as seen in the hyperspectral cube of the target with the reference pixel/spectrum selected *a priori*, the algorithm evaluates an angle  $\theta$  that represents the angular separation between the vector of the mean spectrum of the reference pixels ( $y_i$ ) and the vector representing each pixel's spectrum ( $x_i$ ) in the data space.  $\theta$  is computed as:

$$\theta = \cos^{-1} \left[ \frac{\sum_{i=1}^n x_i y_i}{\left( \sum_{i=1}^n x_i^2 \right)^{1/2} \left( \sum_{i=1}^n y_i^2 \right)^{1/2}} \right] \quad (1)$$

Small values of  $\theta$  are indicative of a higher degree of similarity. As recommended by the developers of the SAM clustering technique, we set  $\theta=0.1^\circ$  as the maximum allowed angle value (Adams & Gillespie, 2006).

In this work, we focus on the two cubes showing the highest spatial resolution in the explored data set (Fig. 2). The two cubes selected here cover Dione's anti-Saturnian hemisphere from 27.8°N to 26.5°S and from 210°W to 260°W. The bright wispy stripes present in this portion of Dione's hemisphere are part of the *Padua Chasmata* feature. The RGB combination used for the original VIMS images is:  $\lambda_R=2.003 \mu\text{m}$ ,  $\lambda_G=1.574 \mu\text{m}$  and  $\lambda_B=1.065 \mu\text{m}$ . Table 1 summarizes cubes' main details. SAM application results are shown in Fig. 3, where different terrain units are represented by the same colors used to identify end-member pixels in Fig. 1. Black color indicate those pixels we decided to not include in the classifica-

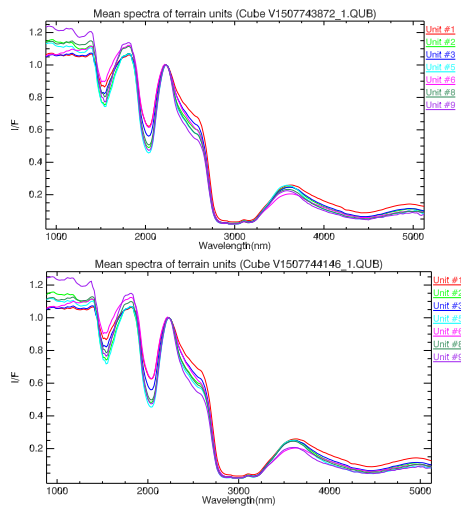


**Fig. 4.** Comparison between the average spectra of terrain units identified for each Dione's VIMS cube.

tion because their spectra show not removable spikes or other faults.

### 3. Results

In Fig. 4 we compare the average spectra of terrain units identified for each cube. The most prominent features are H<sub>2</sub>O ice / OH bands at 1.52, 2.02 and 3.00  $\mu\text{m}$ , while the peak around 3.10  $\mu\text{m}$  is due to Fresnel's reflection in ice grains. Here the dark terraina are represented by units #1 and #6, characterized by a smaller depth of water ice absorptions at 1.5 and 2.0  $\mu\text{m}$  with respect to other units and to the average of the whole satellite, which is indicative of non-ice contaminants on the surface. On the basis of this analysis, it is not possible to clearly identify contaminants features. The nature of the dark terrains of Dione is still debated: Clark et al., (2008) suggests it could be of exogenic origin, caused by charged particles bombardment. The major part of *Padua Chasmata's* bright terrain is categorized in unit #3. Between 0.8 and 1.4  $\mu\text{m}$  its spectrum is similar to that of unit #1, but the absorption features at 1.5 and 2.0  $\mu\text{m}$  are deeper. Unit #3 also classifies the rim and the center of the crater located near the white stripe. In units #2,

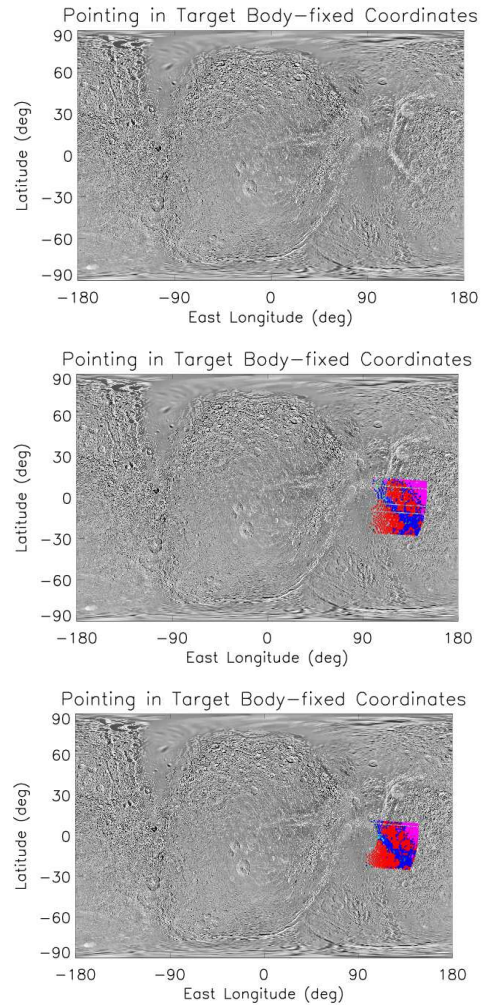


**Fig. 5.** Top: Dione's Map. Middle: Cube V1507743872\_1.QUB projected on Dione's Map. Bottom: Cube V1507744146\_1.QUB projected on Dione's Map

#5, #8 and #9 it is possible to observe spectral signatures due to water ice at 1.04 and 1.25  $\mu\text{m}$ . These units cover just a few percentage of Dione's surface, as can be seen in Table 2, and are confined mainly inside *Padua Chasmata* feature. These absorption bands are well correlated to wispy terrains and could indicate the presence of fresh H<sub>2</sub>O-ice (Stephan et al. 2010). In the other units the latter water ice absorptions are less contrasted or even absent. To

**Table 2.** Terrain units coverage of Dione' surface

Cube	Unit #1 %	units #2 %	units #3 %	units #5 %	units #6 %	units #8 %	units #9 %	Unclassified Pixels
V1507743872_1.QUB	44.5	0.4	26.8	0.1	14.0	0.8	0.1	13.3
V1507744146_1.QUB	57.0	0.7	26.1	0.3	10.5	0.4	0.1	4.9

summarize our results we show the location of the spectral unites inferred from the classification of VIMS infrared spectra, projected onto a map of Dione (Fig. 5). In both cases, classified pixels perfectly fit *Padua Chasmata* and the crater morphology.

#### 4. Conclusions

These results are the first step of a more general PhD work devoted to develop a thermal model of Dione. Given the typical temperatures of the icy Saturnian satellites, the infrared range explored by VIMS does not allow one to retrieve surface temperatures of these bodies including Dione; however, starting from these data it is possible to investigate the compositional and photometric characteristics of the main terrain types. The chemico-physical state of the surface provides a robust boundary condition for

the modeling. Additionally, we plan to model the observed spectral features using radiative transfer theory in order to derive a quantitative evaluation of the contaminants abundance on the surface materials.

#### References

- Adams, J. B., & Gillespie, R., 2006, Remote sensing of Landscapes with spectra images, Cambridge University Press  
 Burch, J. L., et al., 2007, Nature 447, 833  
 Clark, R. N., et al., 2008, Icarus 193, 372  
 Plescia, J. B., & Boyce, J. M., 1982, Nature 295, 285  
 Smith, B. A., et al., 1981, Science 212, 163  
 Stephan, K., et al., 2010, Icarus 206, 631  
 Wagner, R. J., et al., 2005, Bull. Am. Astron. Soc. 37 (3), 701 (Abstr. 36-02)